JOURNAL OF COMPUTATIONAL PHYSICS **124,** 177–191 (1996)
ARTICLE NO. 0052

Low-Dissipation and Low-Dispersion Runge–Kutta Schemes for Computational Acoustics

F. Q. HU,* M. Y. HUSSAINI,† AND J. L. MANTHEY*

*Department of Mathematics and Statistics, Old Dominion University, Norfolk, Virginia 23529 and †Institute for Computer Applications in Science and Engineering, NASA Langley Research Center, Hampton, Virginia 23681

Received December 23, 1994; revised July 26, 1995

In this paper, we investigate accurate and efficient time advancing methods for computational acoustics, where nondissipative and nondispersive properties are of critical importance. Our analysis pertains to the application of Runge–Kutta methods to high-order finite difference discretization. In many CFD applications, multistage Runge–Kutta schemes have often been favored for their low storage requirements and relatively large stability limits. For computing acoustic waves, however, the stability consideration alone is not sufficient, since the Runge–Kutta schemes entail both dissipation and dispersion errors. The time step is now limited by the tolerable dissipation and dispersion errors in the computation. In the present paper, it is shown that if the traditional Runge–Kutta schemes are used for time advancing in acoustic problems, time steps greatly smaller than those allowed by the stability limit are necessary. Low-dissipation and low-dispersion Runge–Kutta (LDDRK) schemes are proposed, based on an optimization that minimizes the dissipation and dispersion errors for wave propagation. Optimizations of both single-step and two-step alternating schemes are considered. The proposed LDDRK schemes are remarkably more efficient than the classical Runge–Kutta schemes for acoustic computations. Moreover, low storage implementations of the optimized schemes are discussed. Special issues of implementing numerical boundary conditions in the LDDRK schemes are also addressed.

1. INTRODUCTION

Computational acoustics is a recently emerging tool for acoustic problems. In this approach, the acoustic waves are computed directly from the governing equations of the compressible flows, namely, the Euler equations or the Navier–Stokes equations. Special needs of numerical schemes for computational acoustics have been indicated in recent works (e.g., [9, 12]). It has been recognized that numerical schemes that have minimal dispersion and dissipation errors are desired, since the acoustic waves are nondispersive and nondissipative in their propagation. In this regard, it has appeared that high-order schemes would be more suitable for computational acoustics than the lower-order schemes since the former are usually less dispersive and less dissipative. Recently, high-order spatial discretization schemes have gained considerable interests in computational acoustics, among them the explicit DRP [12], implicit (or compact) [8, 11], and ENO schemes [6]. In this paper, we investigate accurate and efficient time-advancing schemes for computational acoustics. In particular, the family of Runge–Kutta methods is considered. The present analysis pertains to the application of Runge–Kutta methods to high-order finite difference schemes.

In many CFD applications, popular time-advancing schemes are the classical third- and fourth-order Runge–Kutta schemes because they provide relatively large stability limits [10]. For acoustic calculations, however, the stability consideration alone is not sufficient, since the Runge–Kutta schemes retain both dissipation and dispersion errors. The numerical solutions need to be *time accurate* to resolve the wave propagation. In this paper, we show that when the classical Runge–Kutta schemes are used in wave propagation problems using high-order spatial finite difference, time steps much smaller than those allowed by the stability limit are necessary in the long-time integrations. This certainly undermines the efficiency of the classical Runge–Kutta schemes.

Runge–Kutta schemes are multistage methods. Traditionally, the coefficients of the Runge–Kutta schemes are chosen such that the maximum possible order of accuracy is obtained for a given number of stages. However, it will be shown that it is possible to choose the coefficients of the Runge–Kutta schemes so as to minimize the dissipation and dispersion errors for the propagating waves, rather than to obtain the maximum possible formal order of accuracy. The optimization also does not compromise the stability considerations. The optimized schemes will be referred to as low-dissipation and low-dispersion Runge–Kutta (LDDRK) schemes. Consequently, remarkably larger time steps can be used in the LDDRK schemes, which therefore increases the efficiency of the computation. The optimized four-, five- and six-stage schemes are proposed in the present paper. In addition, optimized two-step schemes are also given in which different coefficients are used in the alternating steps. It is found that when two steps are coupled for optimization, the dispersion and

0021-9991/96 $18.00

dissipation errors can be further reduced and a higher formal order of accuracy can be retained.

Optimization of numerical schemes for wave propagation problems has been conducted in several recent studies (e.g., [8, 12, 16]). In [12], an Adams–Bashforth-type multistep time integration scheme was optimized for acoustic calculations. In that work, the optimization was carried out to preserve the numerical frequency in the development of dispersion-relation-preserving finite difference schemes. In [16], a six-stage Runge–Kutta scheme was optimized for linear wave propagation. Most recently, optimization of five-stage Runge–Kutta schemes was considered in [8] for long-time integration, in which optimized coefficients were given, depending on the spectrum of the initial condition. There are, however, differences between the present and previous works in several aspects. First, the optimization of time advancing is separate from the spatial discretization schemes. The optimization is done once and for all. The proposed LDDRK schemes are applicable to different spatial discretization methods. Second, the optimization is carried out only for the resolved wavenumbers in the spatial discretization. It will be shown that LDDRK schemes preserve the frequency in the time integration and thus are dispersion relation preserving in the sense of [12]. Third, optimizations of two coupled Runge–Kutta steps are considered for the first time. Our results indicate that the two-step schemes offer better properties and are more efficient than the optimized single-step schemes.

The advantages of Runge–Kutta methods also include low storage requirements in their implementations, as compared to Adams–Bashforth-type multistep methods. The low storage requirement is important for computational acoustics applications where large memory use is expected. In the past, it has been shown that the three-stage third-order scheme can be implemented with only two levels of storage. Recently, the fourth-order scheme has been put into a two-level format using five stages in [4]. We point out that, in light of recent studies, most of the LDDRK schemes proposed here can be implemented with two levels of storage, since the number of stages is larger than the formal order of accuracy retained in all schemes except one.

The rest of the paper is organized as follows. In Section 2, the results of Fourier analysis of high-order finite difference schemes are reviewed briefly. Then, time advancing with Runge–Kutta methods is described in Section 3, in which the dissipation and dispersion errors are analyzed using the notion of an amplification factor. The optimization process and LDDRK schemes are given in Section 4 and low-storage implementations are discussed in Section 5. Special issues of implementing boundary conditions are discussed in Section 6. Section 7 contains the conclusions.

2. FOURIER ANALYSIS OF HIGH-ORDER SPATIAL DISCRETIZATION

In this section, the results of Fourier analysis of high-order finite difference schemes are reviewed briefly [14]. For simplicity of discussion, we consider the convective wave equation

$$\frac{\partial u}{\partial t} + c\frac{\partial u}{\partial x} = 0. \tag{2.1}$$

Let the spatial derivative be approximated by a central difference scheme with a uniform mesh of spacing Δx as

$$\left(\frac{\partial u}{\partial x}\right)_j = \frac{1}{\Delta x}\sum_{l=-N}^{N} a_l u_{j+l} \tag{2.2}$$

in which a central difference stencil has been used. In (2.2) u_j represents the value of u at $x = x_j$ and the a_l are the coefficients of the difference scheme. Applying the spatial discretization (2.2) to (2.1), a semi-discrete equation is obtained as

$$\frac{\partial u_j}{\partial t} + \frac{c}{\Delta x}\sum_{l=-N}^{N} a_l u_{j+l} = 0$$

at interior points. Using Fourier analysis, it is easy to show that the semi-discrete equation yields

$$\frac{\partial \tilde{u}}{\partial t} + \mathbf{i}ck^*\tilde{u} = 0, \tag{2.3}$$

where $\tilde{u}$ is the spatial Fourier transform of u and k^* is an effective wavenumber:

$$k^* = \frac{-\mathbf{i}}{\Delta x}\sum_{l=-N}^{N} a_l e^{\mathbf{i}lk\Delta x}, \tag{2.4}$$

k is the actual wavenumber, and $\mathbf{i} = \sqrt{-1}$.

Thus k^* of (2.4) is seen as an approximation to the actual wavenumber k. Moreover, we note that the nondimensionalized effective wavenumber $k^*\,\Delta x$ as a function of $k\,\Delta x$ is a property of the finite difference scheme, depending only on the coefficients of the scheme a_l. (Similar analysis can also be performed for implicit finite difference

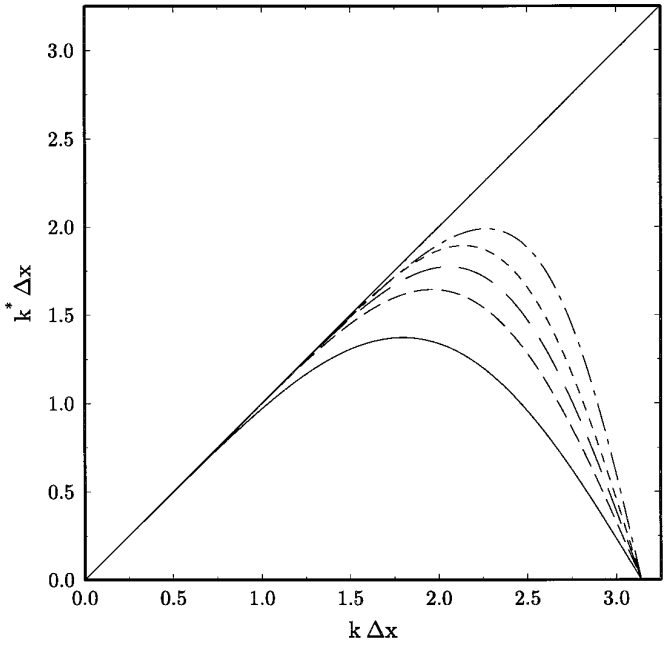

FIG. 1. Numerical wave number $k^* \Delta x$ versus the actual wave number $k \Delta x$ for several high-order finite difference schemes. ——— 5-point 4th-order [7]; – – – 7-point 4th-order [13]; — — — 9-point 6th-order; - - - 11-point 6th-order; – – – 5-point compact [11].

schemes, such as the compact schemes [8, 11]). In Fig. 1, $k^* \Delta x$ as a function of $k \Delta x$ is plotted for several high-order spatial discretization schemes. It is observed that $k^* \Delta x$ approximates $k \Delta x$ adequately for only a limited range of the long waves. For convenience, the maximum resolvable wavenumber will be denoted by k_c^*. Using the criterion $|k^* \Delta x - k \Delta x| < 0.005$, a list of $k_c^* \Delta x$ values for high-order central difference schemes is given in Table I. Often the ''resolution'' of spatial discretization is represented by the minimum points-per-wavelength needed to reasonably resolve the wave. Here the points-per-wavelength value will be computed as $2\pi/k_c^* \Delta x$.

TABLE I

Values of $k_c^* \Delta x$ and $k_{\max}^* \Delta x$ for Several High-Order Central Difference Schemes of the Spatial Derivative

Spatial discretization	$k_c^* \Delta x$	Resolution (points-per-wavelength)	$k_{\max}^* \Delta x$
5-point 4th-order [7]	0.7	9.0	1.4
7-point 4th-order [13][a]	1.16	5.4	1.65
9-point 6th-order[a]	1.31	4.8	1.77
11-point 6th-order[a]	1.48	4.2	1.9
5-point 6th-order compact [11]	1.36	4.6	2.0

[a] The scheme has been optimized to have maximum $k_c^* \Delta x$.

Also listed in Table I are the values of maximum effective wavenumber $k_{\max}^* \Delta x$. The value of $k_{\max}^* \Delta x$ affects the stability considerations, as will be seen below. Clearly, when finite difference schemes are used for the spatial discretization, only the long waves (i.e., for $k \leq k_c^*$) are resolved within a given accuracy.

3. TIME ADVANCING WITH RUNGE–KUTTA SCHEMES

We now consider the time advancing schemes. In particular, the Runge–Kutta methods will be considered in the present paper. For convenience of discussion, a general explicit Runge–Kutta scheme is described below. Let the time evolution equation be written as

$$\frac{\partial \mathbf{U}}{\partial t} = F(\mathbf{U}) \tag{3.1}$$

in which $\mathbf{U}$ represents the vector containing the solution values at spatial mesh points and the operator F contains the discretization of spatial derivatives. For simplicity, we shall assume that F does not depend on t explicitly.

An explicit, p-stage Runge–Kutta scheme advances the solution from time level $t = t_n$ to $t_n + \Delta t$ as

$$\mathbf{U}^{n+1} = \mathbf{U}^n + \sum_{i=1}^{p} w_i \mathbf{K}_i, \tag{3.2}$$

where

$$\mathbf{K}_i = \Delta t\, F(\mathbf{U}^n + \sum_{j=1}^{i-1} \beta_{ij} \mathbf{K}_j), \quad i = 1, 2, ..., p. \tag{3.3}$$

In the above, w_i and β_{ij} are constant coefficients of the particular scheme.

The choice of the time step Δt is an important issue in the Runge–Kutta schemes. One criterion for the time step is that the time integration be stable. The time integration would be considered as stable if the step size is limited by the stability boundary, usually from the ''foot print'' of the particular Runge–Kutta scheme. For references, the stability ''foot prints'' of the classical third- and fourth-order Runge–Kutta schemes are shown in Fig. 2 in the complex $\lambda \Delta t$ plane, where λ is the eigenvalue of the linearized operator of $F(\mathbf{U})$ in (3.1).

To get time accurate solutions, however, the time step Δt is now limited by the tolerable dissipation and dispersion errors, in addition to the stability considerations. Consider, for example, the semi-discrete equation (2.3) of the convective wave equation (2.1) and suppose that the classical fourth-order Runge–Kutta scheme is used. Here, the eigenvalue is $-\mathbf{i}ck^*$ and k^* is real for central difference

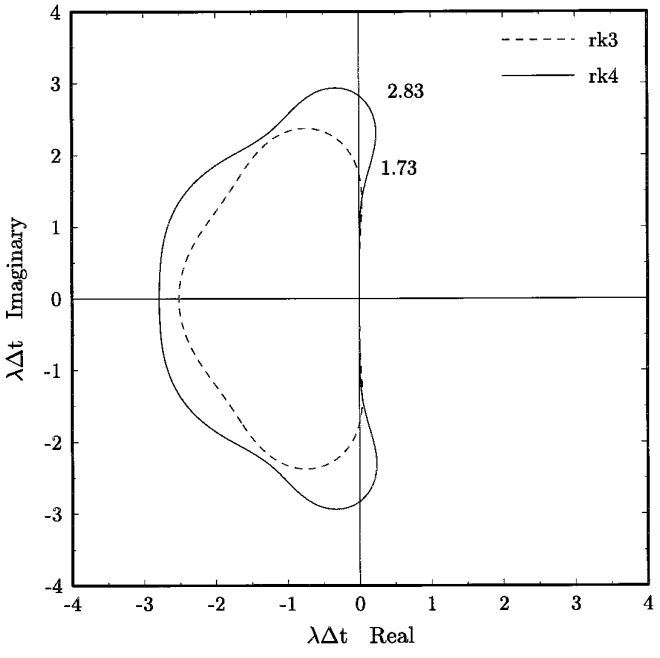

FIG. 2. Stability foot-prints of the third-order (rk3) and fourth-order (rk4) schemes. λ is the eigenvalue of the linearized operator F in (3.1). Indicated are the stability limits on the imaginary axis.

schemes. Thus, from Fig. 2, the fourth-order Runge–Kutta scheme should be stable if Δt is chosen such that

$$ck^*_{\max}\,\Delta t \le 2.83$$

in which $k^*_{\max}$ is the maximum effective wavenumber of the spatial difference scheme. Figure 3 shows the computational results of the convective wave equation, where several different values of Δt have been used, i.e., $ck^*_{\max}\,\Delta t = 2.83, 2.0, 1.0$. In these calculations, the initial value when $t = 0$ is a Gaussian profile $u_0 = 0.5e^{-(\ln 2)(x/3)^2}$ and the wave speed $c = 1$. We take $\Delta x = 1$. Numerical results at $t = 400$ are shown. Since our purpose is to demonstrate the time integration schemes, a nine-point central difference scheme has been used for the spatial discretization in the calculations presented. The exact solution at $t = 400$ is a translated Gaussian profile centered at $x = 400$. The numerical solutions, however, exhibit serious dissipation and dispersion errors for the first two cases. This example shows that, to get time accurate solutions, time steps much smaller than that allowed by the stability limit are necessary when the classical Runge–Kutta schemes are used.

To analyze the numerical errors in the Runge–Kutta schemes, we consider the amplification factor of the schemes, i.e., the ratio of the numerical solution at time levels $n + 1$ and n in the wavenumber domain. From the semi-discrete equation (2.3), it is easy to find that the Runge–Kutta scheme leads to

$$\tilde{\mathbf{U}}_k^{n+1} = \tilde{\mathbf{U}}_k^n \left(1 + \sum_{j=1}^{p} c_j(-\mathbf{i}ck^*\,\Delta t)^j\right)$$

in which c_j are constants related to the coefficients in (3.2) and (3.3). (The specific relations are given later.) $\tilde{\mathbf{U}}_k^n$ is the spatial Fourier transform of $\mathbf{U}^n$. This yields a numerical amplification factor

$$r = \frac{\tilde{\mathbf{U}}_k^{n+1}}{\tilde{\mathbf{U}}_k^n} = 1 + \sum_{j=1}^{p} c_j(-\mathbf{i}\sigma)^j, \tag{3.4}$$

where $\sigma = ck^*\,\Delta t$. The *exact* amplification factor, on the other hand, is found to be

$$r_e = e^{-\mathbf{i}ck^*\,\Delta t} = e^{-\mathbf{i}\sigma}. \tag{3.5}$$

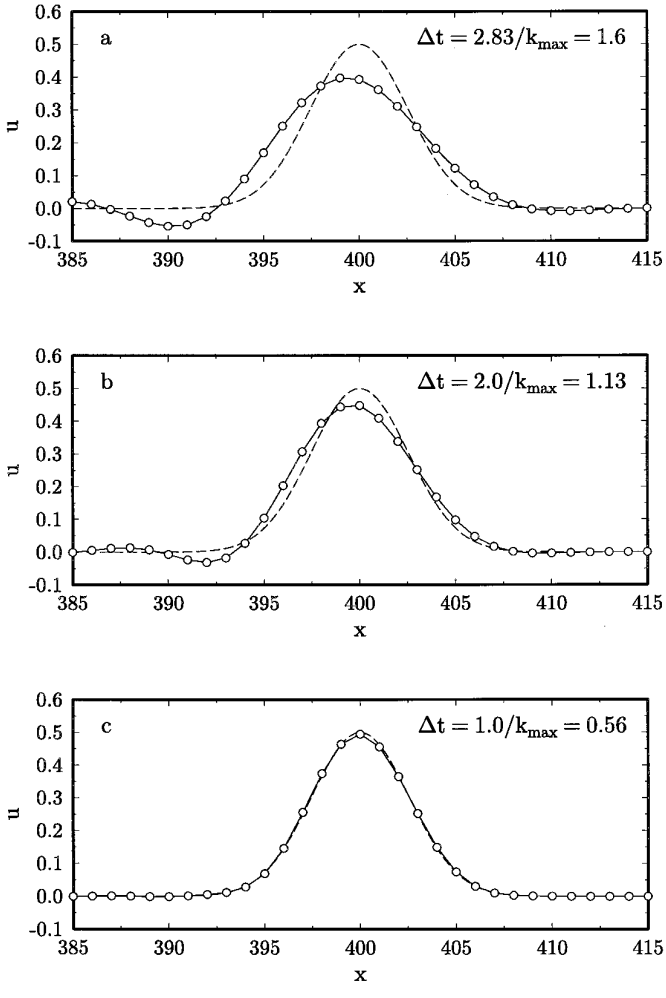

FIG. 3. Numerical examples of the convective wave equation $\partial u/\partial t + \partial u/\partial x = 0$. The classical four-stage fourth-order Runge–Kutta scheme is used. A nine-point central difference scheme has been used for the spatial discretization: ------, exact; —○—, numerical; $t = 400$.

The numerical amplification factor r in (3.4) is seen as a polynomial approximation to the exact factor $e^{-\mathbf{i}\sigma}$. In fact, the order of a Runge–Kutta scheme is indicated by the number of leading coefficients in (3.4) that match the Taylor series expansion of $e^{-\mathbf{i}\sigma}$. For instance, the classical four-stage fourth-order Runge–Kutta scheme has the coefficients $c_1 = 1, c_2 = 1/2!, c_3 = 1/3!, c_4 = 1/4!$. Consequently, the maximum possible order of a p-stage scheme is p (at least in linear cases).

To compare the numerical and exact amplification factors, we express the ratio r/r_e as

$$\frac{r}{r_e} = |r|e^{-\mathbf{i}\delta}. \tag{3.6}$$

In this expression, $|r|$ represents the dissipation rate (or the dissipation error), where the exact value should be 1, and δ represents the phase error (or the dispersion error), where the exact value should be 0. It is easily seen from (3.4) that $|r|$ and δ are functions of $ck^* \Delta t$. Furthermore, they are properties of the given Runge–Kutta scheme and depend only on the coefficients of the scheme. The dissipation rate $|r|$ and the dispersion error δ of the classical third- and fourth-order Runge–Kutta scheme are plotted in Fig. 4. Only the values for positive $ck^* \Delta t$ are shown, since $|r|$ and δ are even and odd functions, respectively. Using the criteria, say, that $||r| - 1| \le 0.001$ and $|\delta| \le 0.001$, it is found that the numerical solution would be *time accurate* for $ck^* \Delta t \le 0.5$ and $ck^* \Delta t \le 0.67$ in the third- and fourth-order Runge–Kutta schemes, respectively.

Following the above analysis, we let R denote the *stability limit* of $ck^* \Delta t$; i.e., the scheme is stable for $ck^* \Delta t \le R$, and we let L denote the *accuracy limit*; i.e., the solution is time accurate for $ck^* \Delta t \le L$. Then, it is necessary for the time advancing scheme to be both stable for *all* wavenumbers and accurate for *resolved* wavenumbers. These considerations lead to the following conditions of determining Δt for the convective wave equation:

$$ck_c^* \Delta t \le L \tag{3.7a}$$

$$ck_{\max}^* \Delta t \le R. \tag{3.7b}$$

That is, in nondimensional terms,

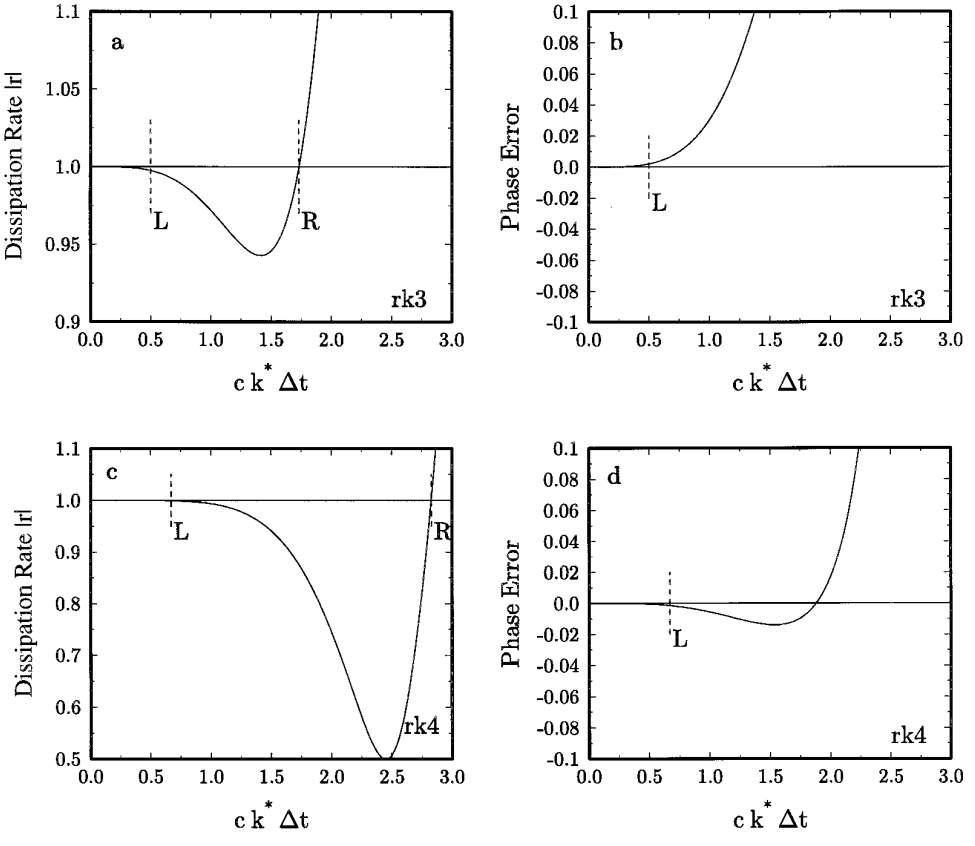

FIG. 4. Dissipation and phase errors of the classical three-stage third-order (rk3) and four-stage fourth-order (rk4) Runge–Kutta schemes. L and R are the accuracy and stability limits, respectively.

$$c\frac{\Delta t}{\Delta x} = \min\left(\frac{L}{k_c^*\,\Delta x}, \frac{R}{k_{\max}^*\,\Delta x}\right). \tag{3.8}$$

Thus, the accuracy limit would give a smaller time step whenever

$$\frac{L}{R} < \frac{k_c^*}{k_{\max}^*}.$$

The above is usually true for the classical Runge–Kutta schemes with the high-order finite differences in which k_c^* is not too much smaller than $k_{\max}^*$ (Table I).

4. LOW-DISSIPATION AND LOW-DISPERSION RUNGE–KUTTA SCHEMES

4.1. *Minimizing the Dissipation and Dispersion Errors*

To optimize the Runge–Kutta schemes, we modify the coefficients c_j in the amplification factor (3.4) such that the dissipation and the dispersion errors are minimized and the accuracy limit L is extended as much as possible. This is in contrast to the traditional choice of c_j that maximizes the possible order of accuracy. The optimized schemes will be referred to as low-dissipation and low-dispersion Runge–Kutta (LDDRK) schemes. In this paper, the optimization is carried out by minimizing $|r - r_e|^2$ as a function of $ck^*\,\Delta t$. It can be shown that this minimizes the approximate sum of the dissipation and dispersion errors (see Appendix A). In addition, a certain formal order of accuracy of the scheme is retained in the optimization process. Thus, the coefficients c_j will be determined, initially, such that the following integral is a minimum:

$$\int_0^\Gamma \left|1 + \sum_{j=1}^{p} c_j(-\mathbf{i}\sigma)^j - e^{-\mathbf{i}\sigma}\right|^2 d\sigma = \text{MIN}, \tag{4.1}$$

where Γ specifies the range of $ck^*\,\Delta t$ in the optimization. This leads to a simple constrained minimum problem which yields a linear system for c_j. However, since the stability condition $|r| \le 1$ is not imposed explicitly in minimizing (4.1), the initial optimized schemes are found to be weakly unstable ($1 < |r| < 1.001$) for some narrow region of the wavenumber. The coefficients, then, are modified slightly by a perturbation technique so that $|r| \le 1$ is satisfied within the given stability limit. Once the values of c_j have been determined, the actual coefficients of the Runge–Kutta schemes, i.e., w_i and β_{ij}, can be found accordingly. Specific implementation will be discussed in Section 5. This optimization process can also be viewed as preserving the frequency (Appendix B) and, thus, is dispersion-relation-preserving in the sense of [12].

Optimizations of four-, five-, and six-stage schemes have been carried out. At least second-order accuracy has been retained; i.e., $c_1 = 1$ and $c_2 = \frac{1}{2}$ for all the schemes and fourth-order accuracy has been retained in the optimized six-stage schemes. The optimized coefficients are given in Table II. Also listed are the respective accuracy and stability limits of the optimized schemes. The accuracy limits L are determined using the criteria $||r| - 1| \le 0.001$ and $|\delta| \le 0.001$. The value of Γ used in (4.1) has been varied such that the accuracy limit L is as large as possible. The dissipation and dispersion errors of the optimized schemes are plotted in Fig. 5. Plotted in dotted lines are the errors of unoptimized scheme in which the coefficients c_j equal those of the Taylor expansion of $e^{-\mathbf{i}\sigma}$.

TABLE II

Optimized Coefficients for the Amplification Factor (3.4)

Stages	c_3	c_4	c_5	c_6	L	R
4	0.162997	0.0407574	—	—	0.85	2.85
5	0.166558	0.0395041	0.00781071	—	1.35	3.54
6	1/3!	1/4!	0.00781005	0.00132141	1.75	1.75

Note. L and R are the accuracy and stability limits, respectively. All the schemes have at least second-order formal accuracy; i.e., $c_1 = 1$, $c_2 = \frac{1}{2}$.

Table II shows that the optimized five-stage scheme can be more efficient than the four-stage scheme, as the increase in the accuracy limit outweighs the cost of the additional stage incurred. On the other hand, the optimized six-stage scheme has a smaller stability limit than the five-stage scheme, although the accuracy limit is larger. This scheme, perhaps, is more useful for spectral methods than finite difference methods [3].

4.2. *Optimized Two-Step Alternating Schemes*

In two-step alternating schemes, we consider schemes in which different coefficients are employed in the alternating steps. The advantages of the alternating schemes are that, when two steps are combined in the optimization, the dispersion and the dispersion errors can be further reduced and higher order of accuracy can be maintained.

Let the amplification factors of the first and the second steps be

$$r_1 = 1 + \sum_{j=1}^{p_1} a_j(-\mathbf{i}\sigma)^j \tag{4.2a}$$

$$r_2 = 1 + \sum_{j=1}^{p_2} b_j(-\mathbf{i}\sigma)^j, \tag{4.2b}$$

where p_1 and p_2 are the number of stages of the two steps, respectively. Accordingly, the scheme will be denoted as p_1–p_2 scheme below. It is easy to see that the amplification

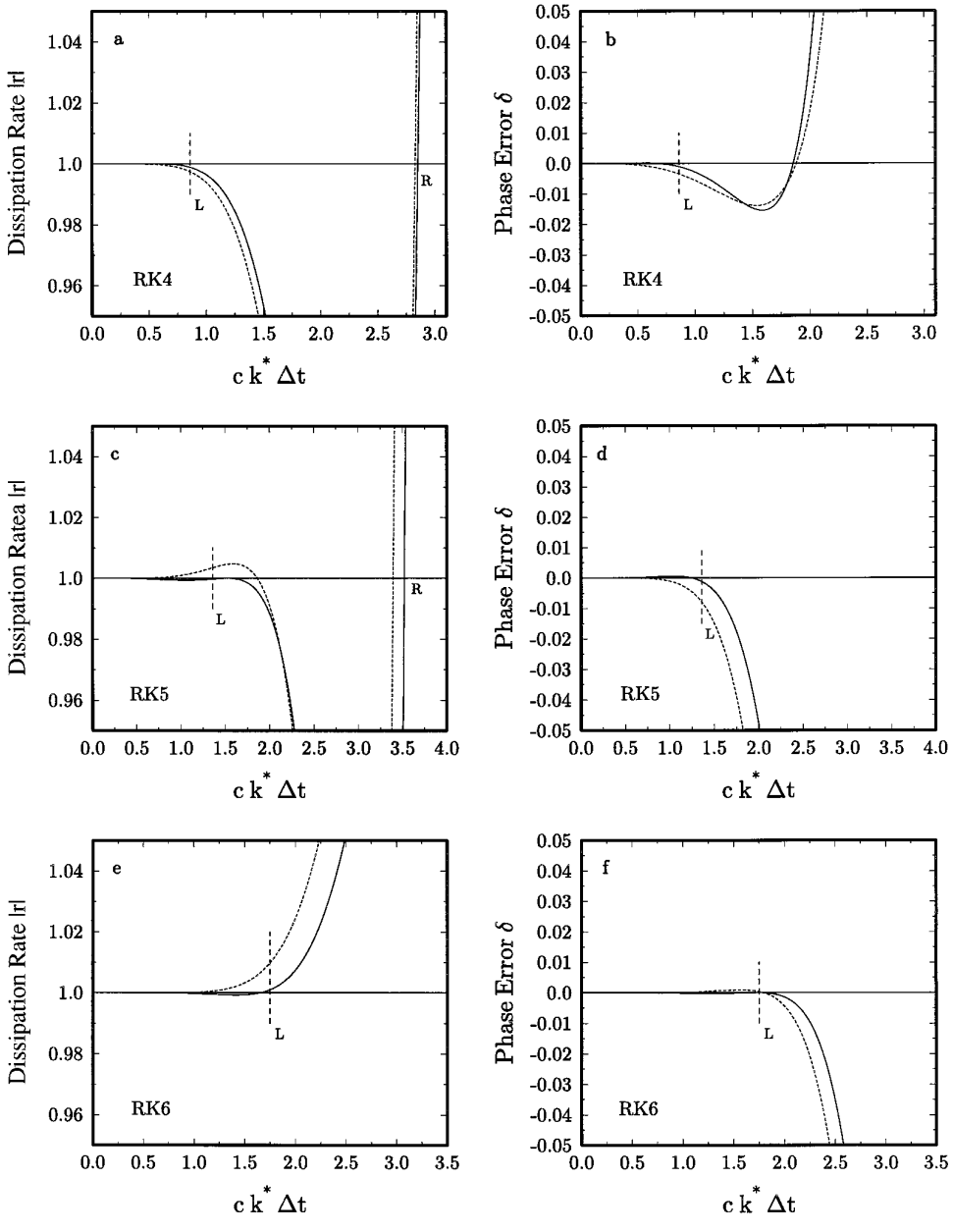

FIG. 5. Dissipation and phase errors of the optimized schemes. Dotted line is the unoptimized scheme: (a) and (b), four-stage; (c) and (d), 5-stage; (e) and (f), 6-stage.

factor for these two steps combined equals $r_1 r_2$. The exact amplification factor, on the other hand, is r_e^2. Again, we now choose the coefficients a_j and b_j such that $|r_1 r_2 - r_e^2|$ is minimized. That is, the coefficients in the alternating steps will be determined such that the following integral is a minimum:

$$\int_0^\Gamma \left| \left(1 + \sum_{j=1}^{p1} a_j (-\mathbf{i}\sigma)^j\right)\left(1 + \sum_{j=1}^{p2} b_j (-\mathbf{i}\sigma)^j\right) - e^{-2\mathbf{i}\sigma} \right|^2 d\sigma = \text{MIN}. \tag{4.3}$$

Optimized coefficients for 4-6 and 5-6 schemes are given in Table III. In both schemes, fourth-order accuracy has been maintained for each step. Thus, the first step in the 4-6 scheme is actually the same as the traditional four-stage fourth-order Runge–Kutta scheme. The dissipation and dispersion errors are shown in Fig. 6 and the stability footprints are given in Fig. 7. For efficiency, we note that the computational cost of the 4-6 alternating scheme is comparable to that of five-stage schemes while that of the 5-6 scheme is slightly higher. However, the 4-6 and 5-6 schemes are fourth-order accurate, whereas

TABLE III

Optimized Coefficients for the 4-6 and 5-6 Schemes of (4.2)

Scheme	Step	Stages	a_5/b_5	a_6/b_6	L	R
4-5	1	4	—	—	1.64	2.52
	2	6	0.0162098	0.00286365		
5-6	1	5	0.00361050	—	2.00	2.85
	2	6	0.0121101	0.00285919		

Note. Fourth-order accuracy has been retained in each step, i.e., $a_1 = b_1 = 1$, $a_2 = b_2 = \frac{1}{2}$, $a_3 = b_3 = \frac{1}{6}$, $a_4 = b_4 = \frac{1}{24}$. L and R are the accuracy and stability limits of each step.

the optimized single-step five-stage scheme is second-order accurate.

Numerical examples of the optimized schemes are shown in Fig. 8, with the same Gaussian initial condition as Fig. 3. By and large, it has been observed that the optimized two-step alternating schemes appear to be more efficient than the single-step optimized schemes.

To further demonstrate the increase in efficiency, we compare the accuracy limits of the optimized and unoptimized schemes, averaged by the number of stages of the scheme in Table IV. The increase in the accuracy limit per stage will result in the increase in the allowable time step when the computational cost is held the same. Here, the optimized 4-6 scheme and 5-6 scheme are counted as 5 and 5.5 stages per time step, respectively. Table IV shows that, for the chosen accuracy, the efficiency of optimized schemes can be as much as twice that of the unoptimized ones. This is found to be consistent with the numerical examples of Figs. 3 and 8. Another example is given in Fig. 9 in which the spherical wave equation,

$$\frac{\partial u}{\partial t} + \frac{\partial u}{\partial r} + \frac{u}{r} = 0,$$

is solved using the optimized 5-6 scheme as well as the unoptimized third- and fourth-order schemes. The time steps, $\Delta t = 0.152$, 0.83, and 1.11 for the optimized 5-6 scheme and the traditional third- and fourth-order schemes, respectively, are chosen such that the total number of stages remains the same in the three calculations. Thus, computational costs are comparable. A boundary condition, $u = \sin((\pi/4)t)$, is applied at $r = 5$ and the wave

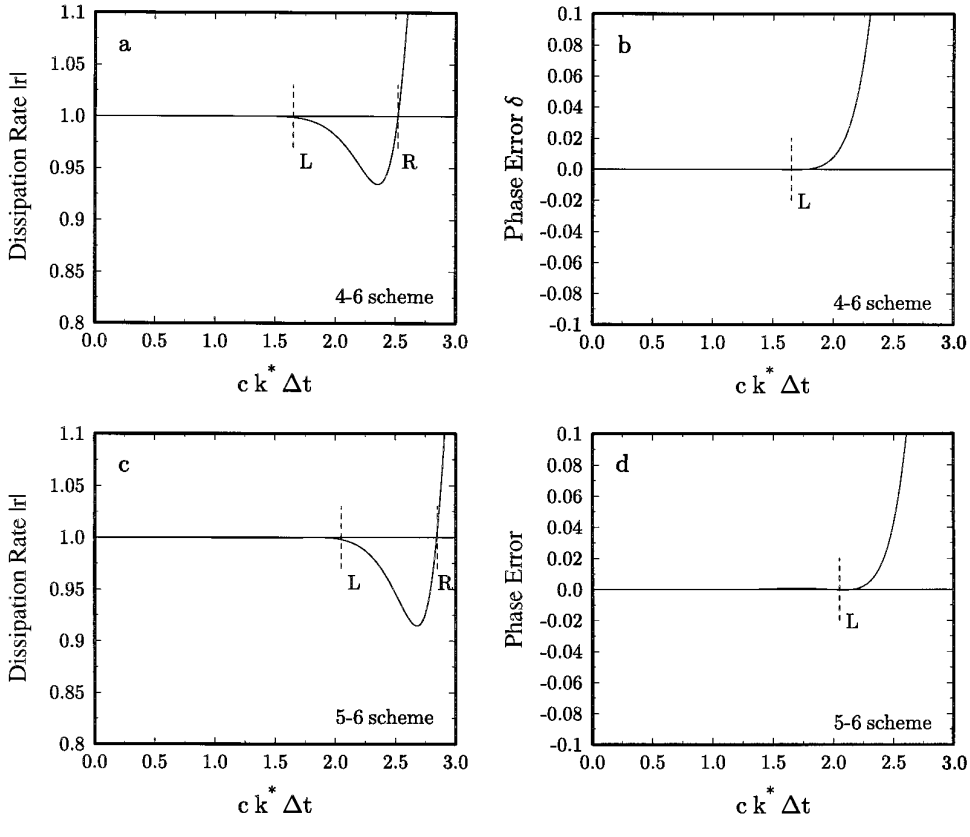

FIG. 6. Dissipation and phase errors of the optimized fourth-order two-step alternating schemes: (a) and (b), 4-6 scheme; (c) and (d), 5-6 scheme.

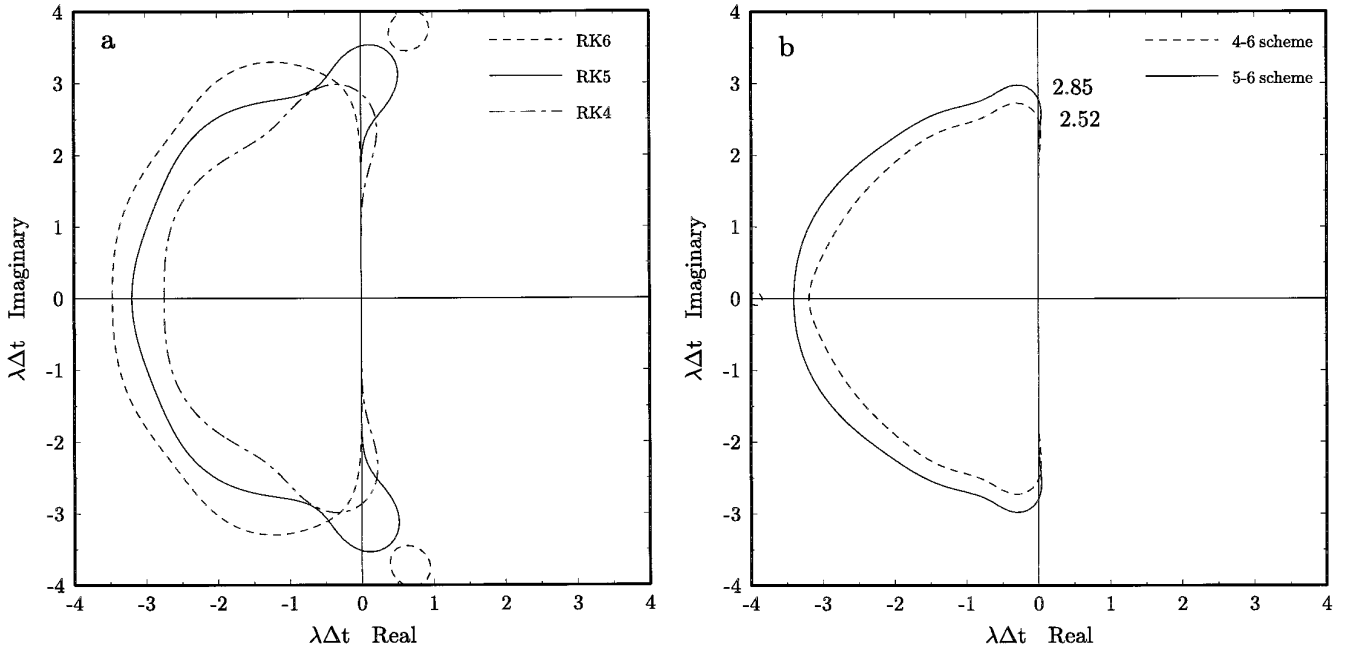

FIG. 7. Stability footprints of the optimized schemes: (a) single step; (b) fourth-order two-step alternating schemes. Indicated are the stability limits on the imaginary axis.

is propagating into the region $r > 5$ with a front at $r = t + 5$. The exact solution is

$$u = \frac{5}{r}\sin\left(\frac{\pi}{4}(t - r + 5)\right) H(t - r + 5),$$

where H is the step function. Numerical results near the wave front are shown in Fig. 9 for $t = 100$, 200, and 300. The dissipation and dispersion errors of the traditional schemes are evident while the results of the 5-6 scheme are more accurate. Consequently, to gain accuracy in this computation, smaller time steps are necessary for the unoptimized schemes, which renders them less efficient.

5. LOW STORAGE IMPLEMENTATION OF LDDRK SCHEMES

In this section, we study the implementation of the LDDRK schemes. Particularly, we will be interested in the implementations that require low memory storages. The low storage requirement is important in computational acoustics applications, where large memory use is expected, especially for 3D problems. In the past, it has been shown that the three-stage third-order Runge–Kutta scheme can be cast in a two-level format but not the four-stage fourth-order schemes [15]. Recently a fourth-order Runge–Kutta scheme has been designed with two levels of storages using five stages [4]. In light of the recent studies, we note that it is possible to implement most of the LDDRK schemes proposed here with two levels of storage, since the number of stages is larger than the formal order of accuracy retained in all schemes except one (namely the 4-6 scheme). The particular implementation of the two-level format, however, will be given elsewhere. In what follows, a low storage implementation of LDDRK schemes for linear problems is outlined.

For linear problems, the following implementation is convenient for a p-stage scheme. Let the time evolution equation be given as (3.1). Then

1. For $i = 1 \cdots p$, compute (with $\overline{\beta}_1 = 0$)

$$\mathbf{K}_i = \Delta t F(\mathbf{U}^n + \overline{\beta}_i \mathbf{K}_{i-1}). \tag{5.1a}$$

2. Then

$$\mathbf{U}^{n+1} = \mathbf{U}^n + \mathbf{K}_p. \tag{5.1b}$$

The coefficients $\overline{\beta}_i$ in (5.1) are related to the coefficients c_j of the amplification factor of LDDRK schemes as follows:

$$\begin{aligned} c_2 &= \overline{\beta}_p \\ c_3 &= \overline{\beta}_p \overline{\beta}_{p-1} \\ &\cdots \\ c_p &= \overline{\beta}_p \overline{\beta}_{p-1} \cdots \overline{\beta}_2. \end{aligned} \tag{5.2}$$

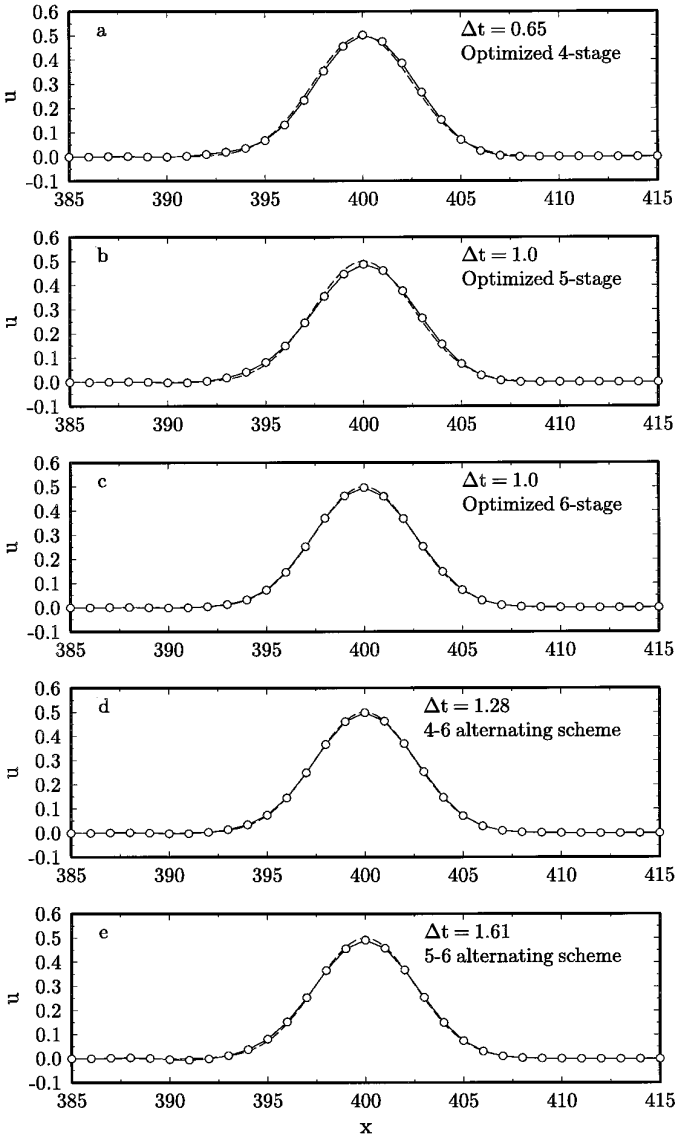

FIG. 8. Numerical examples of the convective wave equation using optimized schemes: ---, exact; —○—, numerical; $t = 400$.

The above scheme can also be applied to nonlinear problems, but it will be formally second-order, in general [3, 10]. This implementation requires at most three levels of storage.

6. IMPLEMENTATION OF BOUNDARY CONDITIONS

The numerical boundary condition is another important issue in computational acoustics. The results of acoustic calculations are particularly sensitive to the errors at the boundary. In this section, the implementations of boundary conditions in Runge–Kutta schemes are discussed. In addition, the implementations of solid wall and radiation boundary conditions are described with an example using the linearized Euler equations.

Often the physical boundary conditions are given in the form of differential equations, such as the characteristics-based boundary conditions or the boundary conditions based on the asymptotic forms of the far field solutions [1, 12]. When boundary conditions are coupled with governing equations of the interior grids, it is not immediately clear as to how the $\mathbf{K}_i$'s in the Runge–Kutta time integration process should be computed at the boundaries.

For simplicity, we assume that the problem is linear or can be linearized at the boundaries. To examine the situation around the boundary grid points, we note that $\mathbf{K}_i$ is related to the time derivatives of the solution $\mathbf{U}$, rather than being some ''intermediate'' value of the solution [5]. Specifically, for the iterations of (5.1) for linear problems, we have

$$
\begin{aligned}
\mathbf{K}_1 &= \Delta t \frac{\partial \mathbf{U}}{\partial t} \\
\mathbf{K}_2 &= \Delta t \frac{\partial \mathbf{U}}{\partial t} + \bar{\beta}_2 \Delta t^2 \frac{\partial^2 \mathbf{U}}{\partial t^2} \\
\mathbf{K}_3 &= \Delta t \frac{\partial \mathbf{U}}{\partial t} + \bar{\beta}_3 \Delta t^2 \frac{\partial^2 \mathbf{U}}{\partial t^2} + \bar{\beta}_3\bar{\beta}_2 \Delta t^3 \frac{\partial^3 \mathbf{U}}{\partial t^3} \\
\mathbf{K}_4 &= \Delta t \frac{\partial \mathbf{U}}{\partial t} + \bar{\beta}_4 \Delta t^2 \frac{\partial^2 \mathbf{U}}{\partial t^2} + \bar{\beta}_4\bar{\beta}_3 \Delta t^3 \frac{\partial^3 \mathbf{U}}{\partial t^3} \\
&\quad + \bar{\beta}_4\bar{\beta}_3\bar{\beta}_2 \Delta t^4 \frac{\partial^4 \mathbf{U}}{\partial t^4} \qquad (6.1) \\
\mathbf{K}_5 &= \Delta t \frac{\partial \mathbf{U}}{\partial t} + \bar{\beta}_5 \Delta t^2 \frac{\partial^2 \mathbf{U}}{\partial t^2} + \bar{\beta}_5\bar{\beta}_4 \Delta t^3 \frac{\partial^3 \mathbf{U}}{\partial t^3} \\
&\quad + \bar{\beta}_5\bar{\beta}_4\bar{\beta}_3 \Delta t^4 \frac{\partial^4 \mathbf{U}}{\partial t^4} + \bar{\beta}_5\bar{\beta}_4\bar{\beta}_3\bar{\beta}_2 \Delta t^5 \frac{\partial^5 \mathbf{U}}{\partial t^5} \\
\mathbf{K}_6 &= \Delta t \frac{\partial \mathbf{U}}{\partial t} + \bar{\beta}_6 \Delta t^2 \frac{\partial^2 \mathbf{U}}{\partial t^2} + \bar{\beta}_6\bar{\beta}_5 \Delta t^3 \frac{\partial^3 \mathbf{U}}{\partial t^3} \\
&\quad + \bar{\beta}_6\bar{\beta}_5\bar{\beta}_4 \Delta t^4 \frac{\partial^4 \mathbf{U}}{\partial t^4} + \bar{\beta}_6\bar{\beta}_5\bar{\beta}_4\bar{\beta}_3 \Delta t^5 \frac{\partial^5 \mathbf{U}}{\partial t^5} \\
&\quad + \bar{\beta}_6\bar{\beta}_5\bar{\beta}_4\bar{\beta}_3\bar{\beta}_2 \Delta t^6 \frac{\partial^6 \mathbf{U}}{\partial t^6} \\
&\cdots
\end{aligned}
$$

The above relations are exact. Thus, it becomes clear that, if $\mathbf{U}$ is known at the boundary, $\mathbf{K}_i$ at the boundary points should be computed according to (6.1). On the other hand, when the boundary condition is given in the form of differential equations, $\mathbf{K}_i$ at the boundary points should be computed from the boundary equations using the *same* Runge–Kutta scheme as at the interior points.

We now discuss the implementation of boundary condi-

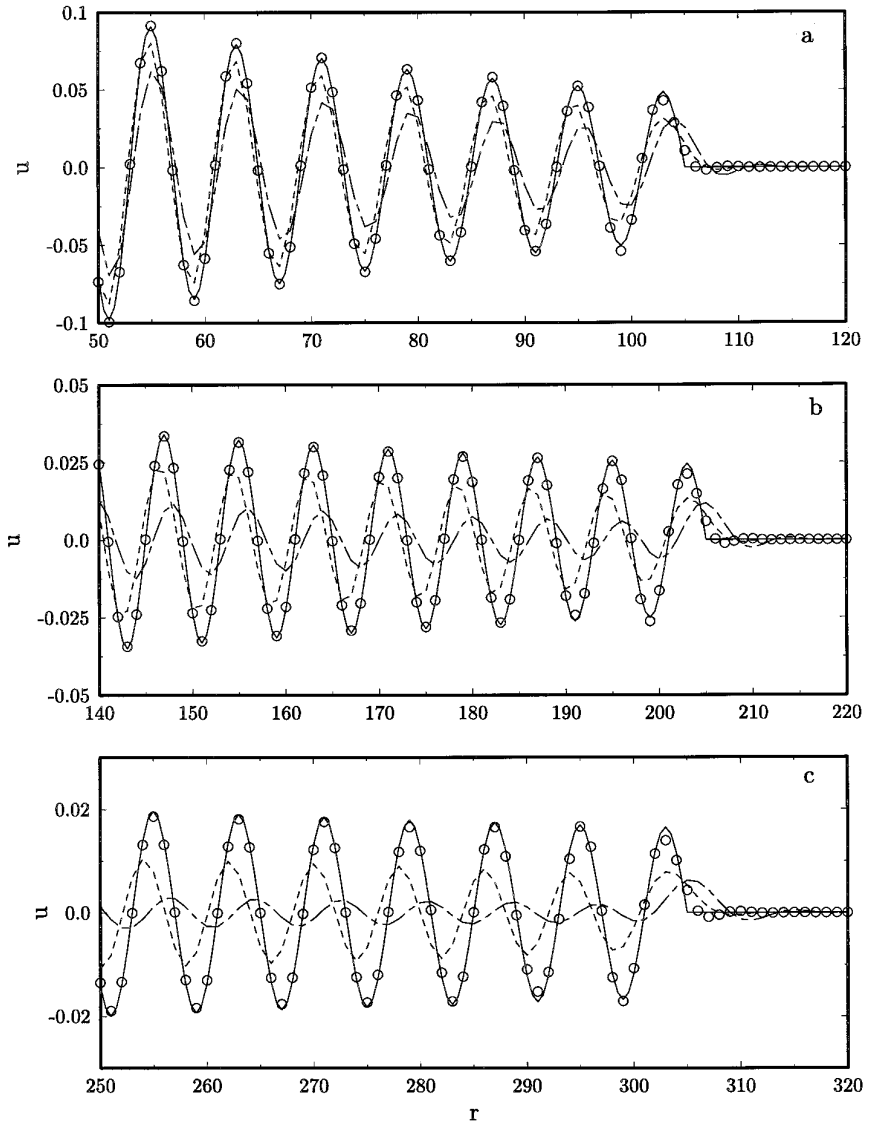

FIG. 9. Numerical results of the spherical wave equation. Plotted are the solutions near the wave front: ———, exact; ○, optimized 5-6 scheme; - - - unoptimized fourth-order scheme; – – – unoptimized third-order scheme. (a) $t = 100$; (b) $t = 200$; (c) $t = 300$.

TABLE IV

A Comparison of Accuracy Limits Divided by the Number of Stages for the Optimized and Unoptimized Schemes

	Unoptimized		Optimized				
Scheme	3rd-order	4th-order	4-stage	5-stage	6-stage	4-6	5-6
L/number of stages	0.17	0.17	0.21	0.27	0.29	0.32	0.36

Note. The accuracy criteria are that the amplitude and phase errors be less than 0.001 as in (3.7a).

tions at the solid walls and the far field for linear acoustic problems. To this end, we consider the linearized Euler equations

$$\frac{\partial \mathbf{U}}{\partial t} + \frac{\partial \mathbf{E}}{\partial x} + \frac{\partial \mathbf{F}}{\partial y} = 0, \tag{6.2}$$

where

$$\mathbf{U} = \begin{pmatrix} \rho \\ u \\ v \\ p \end{pmatrix}, \quad \mathbf{E} = \begin{pmatrix} M_x\rho + u \\ M_x u + p \\ M_x v \\ M_x p + u \end{pmatrix}, \quad \mathbf{F} = \begin{pmatrix} M_y\rho + v \\ M_y u \\ M_y v + p \\ M_y p + v \end{pmatrix}.$$

In the above, ρ, u, v, and p are the density, velocities, and pressure, respectively. M_x and M_y are the Mach numbers of the mean flow in the x and y directions. In what follows, we consider an example of implementing the solid wall and radiation boundary conditions in which the reflection of an acoustic pulse from the solid wall at $y = 0$ is simulated. In this example, we take $M_x = M_y = 0$.

6.1. *Solid Wall Boundary Conditions*

Physically, the boundary condition at a solid wall is that the normal velocity equals zero for inviscid flows. That is, $v = 0$ at $y = 0$. Then, from (6.1), since all the time derivatives of v are also zero, the numerical implementation in the Runge–Kutta schemes should be

$$\mathbf{K}_i = 0 \quad \textit{for the normal velocity components.} \tag{6.3}$$

6.2. *Radiation Boundary Conditions*

The radiation boundary conditions are often derived in the form of differential equations. We consider a radiation boundary condition based on far field asymptotic solutions [1, 12]

$$\frac{\partial \mathbf{U}}{\partial t} = -\frac{\partial \mathbf{U}}{\partial r} - \frac{1}{2r}\mathbf{U}, \tag{6.4}$$

where r is the radial variable.

To couple the radiation condition with the Euler equations in the interior region, (6.4) is integrated for the boundary grids (in the present calculation, three points inward from the boundary) using the same Runge–Kutta time integration scheme as in the interior. The spatial derivatives, however, have to be computed using one-sided differences for the boundary points, where the central difference stencil cannot apply. Specifically, the explicit five-point boundary closure scheme of [7] has been used in the present calculation.

Computational results are shown in Figs. 10 and 11. The initial condition is

$$\rho = p = e^{-(\ln 2)((x^2+(y-25)^2)/9)}, \quad u = v = 0,$$

with $\Delta x = \Delta y = 1$ in nondimensional coordinates. Shown in Fig. 10 are the pressure contours at times $t = 0$, 100, 200, and 300. The spatial discretization is the seven-point central difference scheme [13] and the time integration is the 5-6 LDDRK scheme with $\Delta t = 1.25$. In Fig. 11, profiles of the pressure along the diagonal line $y = x + 200$ are shown for $t = 300$, 400, and 460. The horizontal axis is the distance from the lower left corner of the computational domain. Also shown are the numerical results using the unoptimized third- and fourth-order RK schemes. The time steps used for these two calculations are 0.71 and 0.9, respectively, so that the computer run-times are nearly the same in the three cases. Clearly the optimized scheme gives the most accurate results compared to the exact solution.

7. CONCLUSIONS

An analysis of the dissipation and dispersion properties of the Runge–Kutta time integration methods has been presented for applications with high-order finite difference spatial discretization. Low-dissipation and low-dispersion Runge–Kutta (LDDRK) schemes are proposed, based on an optimization that minimizes the dissipation and dispersion errors for wave propagations. Numerical examples are presented that demonstrate the efficiency and accuracy of the proposed schemes.

The importance of dispersion relations of the finite difference schemes has been emphasized in recent works on computational acoustics. The proposed condition of determining the time step, (3.8), is based on the wave propagation properties of the numerical schemes. It takes account of both the spatial and temporal discretizations. This ensures the correct propagation of resolved waves and, thus, improves the robustness of the computation.

APPENDIX A: DISSIPATION AND DISPERSION ERRORS IN THE AMPLIFICATION FACTOR

Express the complex amplification factor r of (3.4) as $r = |r|e^{-\mathbf{i}\phi}$ and the exact amplification factor $r_e = e^{-\mathbf{i}\sigma}$. Then, for $|\phi - \sigma|$ and $||r| - 1|$ small, which is true in the range of interest in the optimization, we have

$$\begin{aligned} |r - r_e|^2 &= \big||r|e^{-\mathbf{i}\phi} - e^{-\mathbf{i}\sigma}\big|^2 \\ &= \big||r|e^{-\mathbf{i}(\phi-\sigma)} - 1\big|^2 \\ &= \big||r|[1 - \mathbf{i}(\phi - \sigma) + \cdots] - 1\big|^2 \\ &= (|r| - 1)^2 + (\phi - \sigma)^2 + \cdots. \end{aligned}$$

Thus, $|r - r_e|^2$ approximates the sum of the amplitude and phase errors.

APPENDIX B: OPTIMIZATION VIEWED AS PRESERVING THE FREQUENCY

In Section 4, the optimization is carried out by minimizing the difference of the numerical and the exact amplification factors. This actually minimizes the sum of dissipation and dispersion errors as shown in Appendix A. In this appendix, a different view is offered for the optimization process used in Section 4. We show that the minimizing integral (4.1) also preserves the frequency in the time integration. As such the LDDRK scheme is dispersion-relation-preserving in the sense of [12].

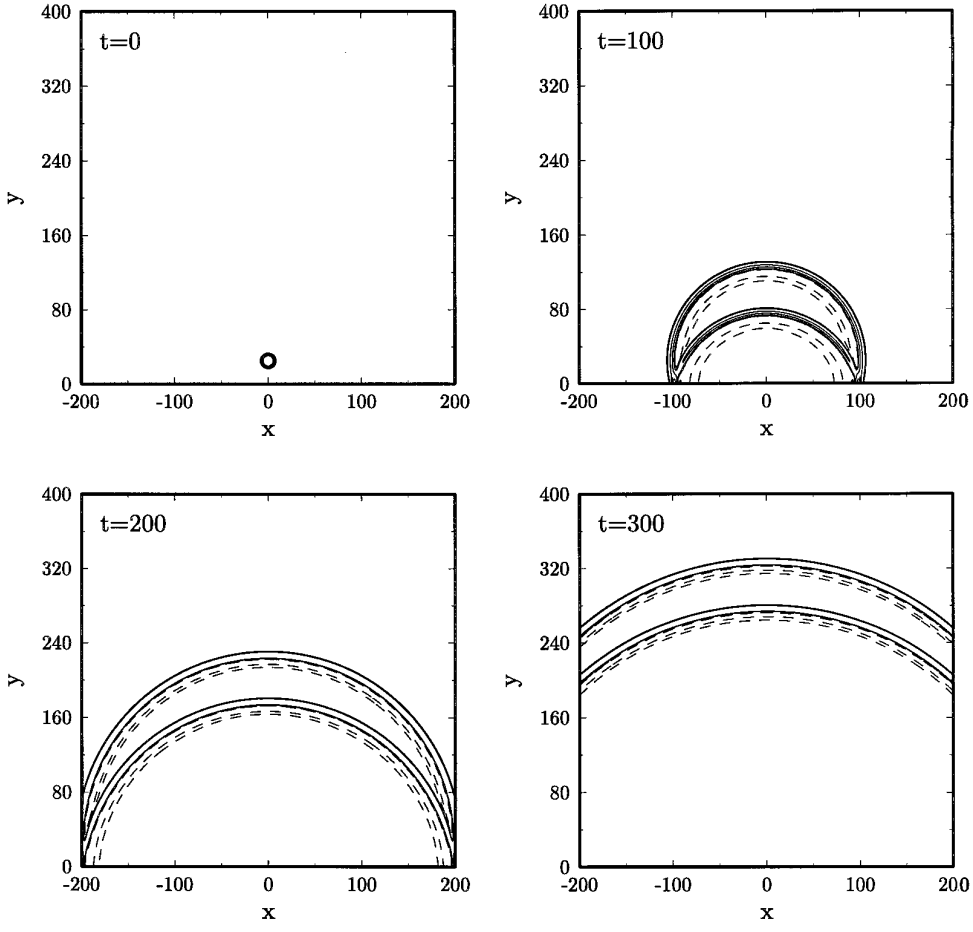

FIG. 10. Numerical examples of an acoustic pulse reflected by a solid wall at $y = 0$. Plotted are the pressure contours at ± 0.1, ± 0.05, ± 0.01, ± 0.005. Numerical boundaries are $x = \pm 200$ and $y = 0$, $y = 400$.

By (6.1) for linearized problems, it is easy to show that the Runge–Kutta scheme leads to

$$\mathbf{U}(t_n + \Delta t) \approx \mathbf{U}(t_n) + c_1 \Delta t \frac{\partial \mathbf{U}}{\partial t}(t_n) + c_2 \Delta t^2 \frac{\partial^2 \mathbf{U}}{\partial t^2}(t_n) + \cdots + c_p \Delta t^p \frac{\partial^p \mathbf{U}}{\partial t^p}(t_n), \tag{B1}$$

where c_i are identical to the coefficients of the amplification factor (3.4). This will be true regardless of the particular form of partial differential equations concerned. The above relation only involves the time derivatives of the solution.

Upon replacing t_n by t and applying Laplace transforms on both sides of (B1), it is found that

LHS,

$$\int_0^\infty \mathbf{U}(t + \Delta t) e^{\mathbf{i}\omega t}\, dt = e^{-\mathbf{i}\omega \Delta t} \tilde{\mathbf{U}}; \tag{B2}$$

RHS,

$$\int_0^\infty \left[\mathbf{U}(t) + c_1 \Delta t \frac{\partial \mathbf{U}}{\partial t}(t) + c_2 \Delta t^2 \frac{\partial^2 \mathbf{U}}{\partial t^2}(t) + \cdots + c_p \Delta t^p \frac{\partial^p \mathbf{U}}{\partial t^p}(t)\right] e^{\mathbf{i}\omega t}\, dt = [1 + c_1(-\mathbf{i}\omega \Delta t) + c_2(-\mathbf{i}\omega \Delta t)^2 + \cdots + c_p(-\mathbf{i}\omega \Delta t)^p]\tilde{\mathbf{U}}, \tag{B3}$$

where $\tilde{\mathbf{U}}$ is the Laplace transform of $\mathbf{U}$ (for simplicity, we assume that $\mathbf{U} = 0$ for $t \le \Delta t$). Next we express

$$1 + c_1(-\mathbf{i}\omega \Delta t) + c_2(-\mathbf{i}\omega \Delta t)^2 + \cdots + c_p(-\mathbf{i}\omega \Delta t)^p \equiv e^{-\mathbf{i}\omega^* \Delta t}. \tag{B4}$$

Equation (B4) equals the amplification factor r in (3.4) when ω is replaced by ck^*. By comparing (B4) and (B2), it is seen that ω^* represents the numerical frequency in the Runge–Kutta time integration scheme. By replacing ck^* with ω in r and r_e, we have

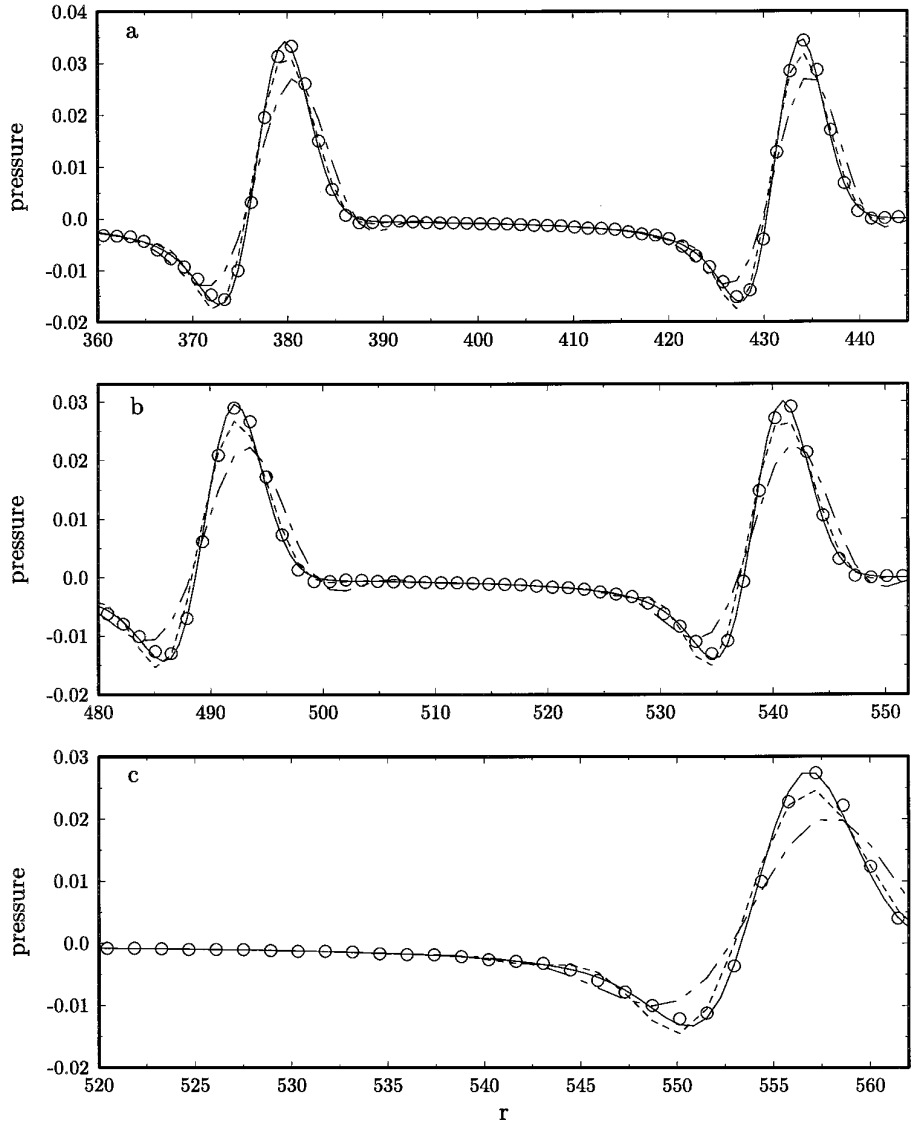

FIG. 11. Pressure profiles along $y = x + 200$. Horizontal axis is the distance from the lower left corner of computational domain; ○, numerical; ———, exact. Also shown are the results of unoptimized schemes, –·– rk3; ·-· rk4. (a) $t = 300$; (b) $t = 400$; (c) $t = 460$.

$$|r - r_e|^2 = |e^{-\mathbf{i}\omega^* \Delta t} - e^{-\mathbf{i}\omega \Delta t}|^2 = |e^{-\mathbf{i}(\omega^* \Delta t - \omega \Delta t)} - 1|^2 \approx |\omega^* \Delta t - \omega \Delta t|^2 \tag{B5}$$

for $|\omega^* \Delta t - \omega \Delta t|$ small. From the above, it is easy to see that the optimization integral (4.1) results in the preservation of the frequency.

ACKNOWLEDGMENTS

The authors were supported by the National Aeronautics and Space Administration under NASA Contract NAS1-19480 while they were in residence at the Institute for Computer Applications in Science and Engineering, NASA Langley Research Center, Hampton, VA 23665.

REFERENCES

1. A. Bayliss and E. Turkel, *Commun. Pure Appl. Math.* **33,** 708 (1980).
2. J. C. Butcher, *The Numerical Analysis of Ordinary Differential Equations, Runge–Kutta and General Linear Methods* (Wiley, New York, 1987).
3. C. Canuto, M. Y. Hussaini, A. Quarteroni, and T. A. Zang, *Spectral Methods in Fluid Dynamics* (Springer-Verlag, New York/Berlin, 1988).
4. M. H. Carpenter and C. A. Kennedy, NASA Technical Memorandum 109112, 1994 (unpublished).
5. M. H. Carpenter, D. Gottlieb, S. Abarbanel, and W.-S. Don, ICASE Report 93-83, 1993 *SIAM J. Sci. Comput.* **16**(6), 1241 (1995).
6. J. Casper, C.-W. Shu, and H. Atkins, *AIAA J.* **32**(10), (1994).
7. J. Gary, *J. Comput. Phys.* **26,** 339 (1978).

8. Z. Haras and S. Ta'asan, *J. Comput. Phys.* **114,** 265 (1994).
9. J. Hardin and M. Y. Hussaini, *Computational Aeroacoustics* (Springer-Verlag, New York/Berlin, 1992).
10. A. Jameson, W. Schmidt, and E. Turkel, AIAA Paper 81-1259, 1981 (unpublished).
11. S. K. Lele, *J. Comput. Phys.* **103,** 16 (1992).
12. C. K. W. Tam and J. C. Webb, *J. Comput. Phys.* **107,** 262 (1993).
13. C. K. W. Tam and H. Shen, AIAA Paper 93-4325, 1993 (unpublished).
14. R. Vichnevetsky and J. B. Bowles, *Fourier Analysis of Numerical Approximations of Hyperbolic Equations* (SIAM, Philadelphia, 1982).
15. J. H. Williamson, *J. Comput. Phys.* **35,** 48 (1980).
16. D. W. Zingg, H. Lomax, and H. Jurgens, AIAA Paper 93-0459, 1993 (unpublished).